ACS NANO

www.acsnano.org

ARTICLE

Macroscopic Alignment of Block Copolymers on Silicon Substrates by Laser Annealing

Arkadiusz A. Leniart, Przemyslaw Pula, Andrzej Sitkiewicz, and Pawel W. Majewski*

Cite This: *ACS Nano* 2020, 14, 4805–4815

Read Online

ACCESS | Metrics & More | Article Recommendations | Supporting Information

ABSTRACT: **Laser annealing is a competitive alternative to conventional oven annealing of block copolymer (BCP) thin films enabling rapid acceleration and precise spatial control of the self-assembly process. Localized heating by a moving laser beam (zone annealing), taking advantage of steep temperature gradients, can additionally yield aligned morphologies. In its original implementation it was limited to specialized germanium-coated glass substrates, which absorb visible light and exhibit low-enough thermal conductivity to facilitate heating at relatively low irradiation power density. Here, we demonstrate a recent advance in laser zone annealing, which utilizes a powerful fiber-coupled near-IR laser source allowing rapid BCP annealing over a large area on conventional silicon wafers. The annealing coupled with photothermal shearing yields macroscopically aligned BCP films, which are used as templates for patterning metallic nanowires. We also report a facile method of transferring laser-annealed BCP films onto arbitrary surfaces. The transfer process allows patterning substrates with a highly corrugated surface and single-step rapid fabrication of multilayered nanomaterials with complex morphologies.**

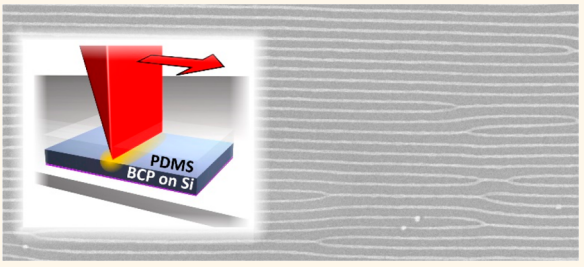

KEYWORDS: *block copolymers, laser annealing, directed self-assembly, multilayers, nanopatterning, photothermal processing*

Block copolymers (BCPs), thanks to their ability to self-assemble into ordered nanometer-scale morphologies, have been long recognized as a convenient synthetic platform for various nanostructured materials.[1] While BCPs have found use as bulk heterogeneous materials, *e.g.*, high-performance elastomers,[2] their anticipated potential lies in solution-based[3] and thin-film applications.[4−7] As thin films, these periodic nanostructures can be utilized as filtration[8−10] and ion-conducting membranes,[11−13] lithography masks,[14−18] and electronic[5,6] and photovoltaic materials.[19−21] Despite numerous efforts, reaching the point when practical implementation of BCP self-assembly can compete with conventional top-down fabrication remains a challenge. It is primarily hindered by impractically slow self-assembly kinetics caused by high viscosity of these materials and by high density of kinetically trapped structural defects present in spontaneously ordered films.[22,23] Typically, spontaneous self-assembly yields only short-range ordered BCP morphologies with grain size not exceeding several repeats of the spacing between the microdomains.[24] The introduction of directing biases during the microphase separation, known as directed self-assembly (DSA), induces long-range order and, frequently, shortens the time of annealing.[25] Currently, the arsenal of DSA techniques is very extensive and includes methods based on physical and chemical interactions.[26−28] The former include utilization of electric[29−33] and magnetic fields,[34−37] mechanical shearing,[38,39] and graphoepitaxy.[40−44] The latter rely on altering chemical interactions between block copolymers and their environment. Notably, chemical epitaxy DSA involves patterned substrates, which induce preferential or neutral wetting of BCP blocks.[19,45−47] Alternatively, self-assembly can be accelerated by lowering BCPs' viscosity by blending them with low molecular weight polymers[48] or other plasticizers such as small molecules during exposure to solvent vapor[49−51] or immersion in a poor solvent.[52,53]

Thermal zone annealing DSA methods utilize nonuniform temperature fields, which, through steep temperature gradients, impose a directional bias on the growth of BCP domains, leading to long-range alignment.[25,54] Depending on the temperature regime of an experiment, "cold zone annealing" (CZA)[54,55] or "hot zone annealing" (HZA)[56−59] can be pursued. In the case of HZA, the ordering and alignment proceed when the polymer is cooled from the isotropic melt through the order−disorder transition temperature, T_{ODT}, resembling directional solidification of crystalline materi-

Received: January 24, 2020
Accepted: March 11, 2020
Published: March 11, 2020

als.[60,61] Cold zone annealing experiments, where the BCP undergoes order−order transition (OOT), have also been reported,[62] but typically, the material is moved across a thermal zone with lower-bound temperature above the T_g, enabling morphological rearrangements, but with upper-bound temperature well below the T_{ODT} or T_{OOT}.[54,55]

Recently, new hybrid zone annealing methods have been proposed. In particular, dynamic sharp temperature gradient zone annealing (S-CZA) proposed by Singh *et al.* exploits morphology-directing shearing effects present when nonstationary, sharp thermal gradients are induced by the movement of a hot wire under the BCP film.[63,64] The shearing caused by thermal expansion effects can be further amplified by application of a soft elastomeric PDMS pad on top of the BCP, leading to large-area uniaxial alignment of cylindrical domains in the heated-zone movement direction in soft-shear CZA (SS-CZA).[65] A nonthermal analogue of this approach is a combination of solvent vapor annealing plasticizing the BCP and soft mechanical shearing caused by swelling and expansion of the PDMS reported by Vogt *et al.*[66] and further explored by Epps and co-workers.[67]

As recently reviewed by Tan and Wiesner[68] and by Nowak and Yager,[69] laser processing of complex structured materials has recently gained momentum as an alternative to conventional processing techniques primarily for its superior spatial control and time efficiency but also due to the advent of affordable high-power laser sources. It has been employed in processing polymeric materials ranging from photoresists and polymeric inks to block copolymers. Laser annealing (LA) experiments, which utilize nonstationary beams, can be effectively classified as zone annealing methods due to the highly localized nature of the photothermally heated zone.[24,70−72] Depending on the power density of laser illumination, the maximum temperatures reached in the experiment may exceed[73−75] or may not reach the T_{ODT} of the material,[24,75] analogous to HZA or CZA, respectively. Laser heating enables very fast ordering of BCP morphologies by providing extremely rapid access to annealing temperatures, which would otherwise irreversibly damage the material during the prolonged exposures.[17,70] Acceleration of grain-growth kinetics and shortening of the annealing duration to mere milliseconds[24,73,74,76] and even to a sub-millisecond regime[68,70] have been reported in photothermal annealing experiments.

More complex laser annealing techniques were proposed; Singer *et al.* have demonstrated how a combination of directional evaporation of residual solvent and a highly localized laser directs the orientation of polymeric micelles in PS-*b*-PDMS thin films.[77] The soft-shear laser zone annealing (SS-LZA) technique stems from SS-CZA utilizing a focused laser line to induce an elongated "hot zone" in the BCP film clad with a thick elastomeric pad.[78−80] Large differences between thermal expansion coefficients of a BCP-supporting substrate and the elastomer induce soft shearing and alignment of BCP morphology. This approach is effective in the alignment of various BCPs provided that the time scales of photothermal shearing are faster than morphological relaxation of the polymer.[78] To achieve efficient photothermal shearing, steep temperature profiles rapidly advancing across the BCP substrates are required. For the alignment of macroscopic samples, line- or ellipse-shaped laser beams are used with the long-axis of the beam oriented perpendicular to the motion direction.[75,78] Such profiles can be induced at relatively low aerial power density of laser illumination (ρ) only in the substrates with low thermal conductivity such as glass or fused silica ($k \approx 1$ W m^{-1} K^{-1}); however the transparency of such substrates to the visible and near-IR photons ($\lambda = 0.4-2.7$ μm) introduces another challenge.[24,75,78] To alleviate this problem, BCP-supporting substrates can be coated with light-absorbing layers, *e.g.*, sputtered germanium (532 nm, 3 W, $\rho_{av} \approx 10$ W mm^{-2})[24] or spin-coated graphene[75] (1064 nm, $\rho_{av} \approx 20$ W mm^{-2}). In addition, the germanium-glass substrates require passivation with a thin layer of silicon nitride if further chemical conversion of the BCP is necessary.[79] Utilization of silicon substrates, which are the gold standard in BCP research, seems to be the natural direction in which laser annealing methods should evolve. It is however quite a difficult task to photothermally heat a macroscopic area of a standard silicon chip (0.5 mm thick) due to the very high thermal conductivity of this material, $k = 148$ W m^{-1} K^{-1}, comparable to that of aluminum alloys[81] and rapid dissipation of the deposited energy. This difficulty can be overcome by decreasing the size of the illuminated spot along with increasing the illumination power density. This approach, with the use of a (532 nm, 350 mW) laser focused with a microscope objective (0.66 μm, Gaussian fwhm, $\rho_{av} \approx 350$ kW mm^{-2}) called focused laser spike (FLASK) annealing, has been demonstrated by Singer and co-workers,[82,83] who also took advantage of the "self-focusing" properties of Si, *i.e.*, the decrease of its thermal conductivity with temperature, which in a positive feedback loop helps the heating. Similarly, Thompson *et al.* have used an ellipse-shaped near-IR beam (980 nm, 60 W, $\rho_{av} \approx 120$ W mm^{-2}) to reach temperatures above the order−disorder transition temperature (700 °C) of a PS-*b*-PMMA BCP.[74]

RESULTS AND DISCUSSION

We present a recent advance in the laser zone annealing method that enables large-area uniaxial alignment of BCP samples on conventional silicon substrates. Our method combines laser heating (980 nm, 30 W laser) with soft shearing, allowing rapid monodomain-type ordering of cylinder-forming polystyrene-*block*-poly(2-vinylpyridine) (PS-*b*-P2VP) block copolymers over a macroscopic area (>2 cm^2) during a few-minutes-long annealing experiment. Photothermal annealing is performed in the *cold-zone* thermal regime, *i.e.*, without crossing the T_{ODT}. We describe the construction of a small-footprint annealing device powered by an industrial fiber-coupled diode laser and characterize its optical parameters and thermal performance. We examine the influence of key BCP processing parameters such as illumination intensity, the duration of annealing, and base temperature on the efficiency of BCP morphology alignment and demonstrate the application of our method in patterning complex BCP motifs on various substrates. Our study also addresses the problems that inadvertently arise in the high-power laser annealing. In particular, we emphasize the necessity of the reproducible thermal-grounding and adequate dissipation of heat from the sample, which prevents uncontrollable bulk heating due to the significant accumulation of energy deposited by the beam.

Figure 1a shows an overview of the two principal elements of our laser annealing setup: the IR diode laser head and the vacuum chamber mounted on a motorized stage. We utilize a 30 W laser with a 980 nm multimode diode emitter dedicated for industrial cutting and engraving applications with custom-built power control. The 980 nm radiation selected for our experiments presents a compromise between the photon absorption depth in silicon (≈ 100 μm),[84] light intensity losses

https://dx.doi.org/10.1021/acsnano.0c00696
ACS Nano 2020, 14, 4805−4815

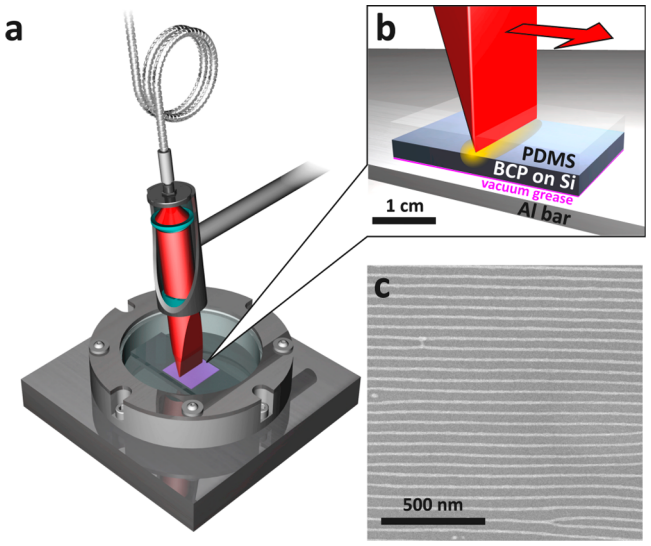

Figure 1. Overview of the compact laser annealing setup. (a) Cutaway view of the optical head shaping the beam into a narrow line with a connected optical fiber. The beam is projected onto a sample inside a low-profile vacuum chamber mounted on a linear translation stage. (b) Block copolymer thin-film sample on a silicon substrate capped with a layer of transparent PDMS undergoing laser annealing in soft-shearing mode (SS-LZA). The line-shaped beam is continuously rastered across the sample with a PDMS cap acting as a shear-inducing element. (c) Metallic platinum nanowires on Si obtained by templated synthesis in the aligned cylindrical PS-*b*-P2VP diblock copolymer film after 8 cycles of photothermal annealing at 0.32 mm s^{-1} with 24 W beam power.

due to reflection ($R \approx 30\%$),[84] and commercial availability of high-power laser diodes. It is worth noting that the 980 nm beam can be detected by an off-the-shelf digital camera, which is very helpful at the stage of alignment and operating the setup.

The use of fiber-optics to deliver the beam to a small cylindrical head with beam-shaping optics renders the setup very compact (<20 cm × 20 cm × 20 cm) and minimizes its overall footprint in a laboratory. Block copolymer samples on silicon substrates are placed on the aluminum baseplate. A thin, 50 μm, layer of high-temperature resistant vacuum grease is used to secure Si chips and to provide thermal contact with the plate. The baseplate is placed inside a low-profile vacuum chamber evacuated to <1 mbar, which prevents oxygen degradation of polymers at high temperatures. The chamber is mounted on a translation stage, enabling controlled bidirectional motion of the substrate. The light emitted by the optical fiber is focused by a set of spherical and cylindrical lenses into a long narrow line oriented perpendicularly to the motion direction (Figure 1b). The BCP films are clad with a transparent layer of cross-linked polydimethylsiloxane (PDMS) elastomer, which due to high coefficient of thermal expansion, imposes shear stress that directionally aligns the underlying BCP morphology.[78] Figure 1c shows an example of an aligned layer of cylinder-forming polystyrene-*b*-poly(2-vinylpyridine) with a total molecular mass of 116 kg mol^{-1} (C116) converted to a platinum nanowire replica[85] after 8 bidirectional passages (cycles) of the laser line at 0.32 mm s^{-1} velocity. The cylinders align parallel to the laser passage direction.

The optical profile of the line at the sample plane shown in Figure 2a,b is approximately 120 μm (fwhm) by 5 mm (fwhm), dictated primarily by the diameter and numerical aperture of the optical fiber (0.22 and 100 μm, respectively), and a ratio of focal lengths of the lenses (more details provided in the Supporting Information). As expected, the optical emission profile of the multimode diode laser is non-Gaussian. After focusing, intensity inhomogeneities (spots) are present in the 2D profile of the laser line (Figure 2a). Due to the resolution of the optical profiler, they are less pronounced in the short-axis profile of the laser line and only manifest as beam-broadening sidebands but are clearly visible along the length of the line (SI Figure S3). These inhomogeneities, however, are mostly suppressed in the resultant thermal profiles due to the high thermal conductivity of silicon (Figure 2c). It should be noted that both PS-*b*-P2VP and PDMS are transparent to 980 nm IR radiation,[86,87] and both are heated indirectly by heat conducted away from the irradiated surface of silicon. Despite poor heat conduction of polymeric materials (~1 W m^{-1} K^{-1}), due to negligible BCP film thickness (<100 nm) and relatively low laser line velocity used here, the variation in temperature of the polymer in the direction normal to the surface can be neglected and assumed to be equal to that of the underlying Si surface.[76] Surface temperature profile

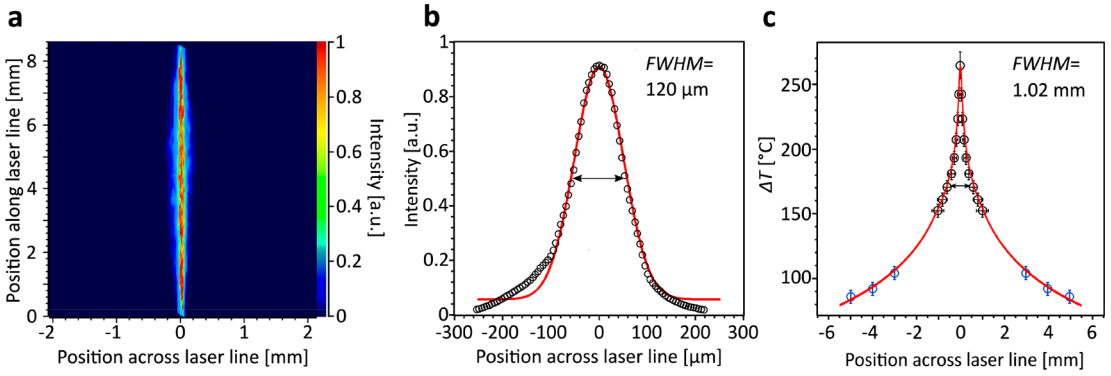

Figure 2. Optical and thermal fields used in laser annealing. (a) 2D optical profile of the laser line recorded at the sample position. (b) Transverse profile of illumination intensity profile, integrated over a 2-mm-wide central portion of the line. A fit to a Gaussian function is shown in red. (c) Silicon surface temperature profile across the laser line at 27 W of incident power recorded in vacuum. Data points obtained by melt-mark analysis and conventional thermocouple measurements are marked by black and blue circles, respectively. The red line is a guide to the eye. Full-width at half-maximum parameters are provided for both optical and thermal profiles.

https://dx.doi.org/10.1021/acsnano.0c00696
ACS Nano 2020, 14, 4805−4815

shown in Figure 2c recorded at 27 W of incident laser power was obtained by combining melt-mark analysis[24] data (SI Figure S4) near the center of the line with conventional thin gauge thermocouple measurements in the far field. The rise in temperature over the ambient value, ΔT, caused by laser illumination, rather than the absolute temperature value, is shown in the plot to facilitate conversion between different power of illumination and changes in absorption due to the presence of an antireflective BCP layer.[88]

Due to the short time scales of heat diffusion ($\approx$ 0.4 s, see eq 3 and Figure S7 in the SI) and fast thermal equilibration, the stationary temperature profile acquired under static beam illumination is closely matching the instantaneous temperature distribution in the sample during steady slow motion (<1 mm s^{-1}) laser sweep.[24] While the thermal history of the sample during each laser sweep can be conveniently obtained from temperature profiles by converting the spatial coordinate to time, it is worth noting that heat dissipation is fast enough to limit heat accumulation over consecutive annealing cycles and bulk sample heating. Therefore, all laser sweeps and annealing cycles performed at constant velocity and laser power are thermally identical.

The width of the thermal zone in Si ($fwhm_{thermal} \approx 1000$ μm) is significantly broader than that previously reported for LZA experiments, which utilized germanium-coated glass substrates (3 W, $fwhm_{optical}$ = 20 μm, $fwhm_{thermal}$ = 92 μm).[24] At the same time, the peak temperature is reduced from 500 °C to 300 °C. The hot zone shapes differ due to several factors: the larger width of the optical profile of the 980 nm laser line, much larger thermal diffusivity of Si (~90 mm^2 s^{-1}) compared to glass (~0.5 mm^2 s^{-1}),[81] and larger depth of penetration for 980 nm (absorption depth z_o = 102 μm)[84] compared to germanium (<100 nm for 532 nm). For the above-mentioned reasons, it is not possible to obtain equally high and steep temperature profiles in Si as in poorly conducting substrates without resorting to much more powerful laser sources. Alternatively, at the expense of the size of the annealing zone, the beam can be focused to a smaller elliptical or circular spot. A quantitative comparison of temperature profiles induced in Si and glass/Ge substrates during laser annealing is presented in SI Figure S11.

Notably, we found that proper thermal grounding, *i.e.*, stable thermal contact between the bottom Si surface and the sample carrier bar, is of primary importance in photothermal annealing experiments. A thin layer of vacuum grease or other thermally stable heatsink compound is necessary to prevent thermal runaways. In contrast to the glass-germanium substrates, where the heat diffusion process is primarily determined by poorly conductive glass,[24] thermal resistance of the grease layer has to be taken into account in high-power laser heating of Si (Section 5 of the SI). To ensure reproducibility of thermal profiles in each laser annealing experiment, we devised a simple tool allowing precise gap-alignment during sample mounting (SI Figure S10).

Temperature gradients are necessary to induce the soft-shearing effect responsible for laser alignment of BCP morphologies both in the hot-[72,75] and cold-zone modes of BCP processing.[78] The in-plane shear stresses accumulate in the locally heated zone at the boundary between two materials with different coefficients of thermal expansion (α_{Si} = 2.57 ppm K^{-1}, α_{PS} = 70 ppm K^{-1}).[89] This effect can be greatly enhanced by the application of a macroscopically thick (~0.5 mm) cross-linked polydimethylsiloxane pad on top of the BCP film (α_{PDMS} = 320 ppm K^{-1}).[90] We have chosen this approach as particularly effective in the cold-zone mode of laser annealing, in which the elastomeric pad transduces shear stresses to the underlying BCP domains. The domains remain in an ordered microphase-separated state throughout the process and align over a macroscopic area in response to shear stresses. Conversely, highly localized hot-zone processing, applicable to systems with accessible T_{ODT}, does not require shear enhancement and was demonstrated to locally guide the BCP patterns.[75]

Due to the thermal properties of silicon outlined above, surface temperature gradients in this work (63 K mm^{-1} at fwhm of the ΔT profile) are more than 1 order of magnitude smaller than those in glass (~10^3 K mm^{-1}).[25] Lower temperature gradients lower the shear stresses in the BCP film, which, in turn, translate to lower shear rates in the dynamic annealing experiments. In our experiments we have tested the influence of high-temperature transients and soft shearing on thin films of PS-*b*-P2VP, the material whose propensity for the SS-LZA alignment has previously been shown to be relatively insensitive to the shear rate.[78] Despite much lower temperature gradients and lower peak temperatures used in the current work, the morphology of cylinder-forming PS-*b*-P2VP BCPs macroscopically aligns in the direction of laser line movement. Figure 1c shows a scanning electron microscope (SEM) image of a well-ordered and highly aligned monolayer-thick film of C116 processed by laser annealing at optimized conditions after conversion to a metallic replica,[91] which clearly demonstrates the utility of our approach. It has been previously shown that PS-*b*-P2VP is quite insensitive to the shear rate employed in photothermal processing and responds by morphology alignment in soft-shearing experiments performed over a broad range of laser sweep velocities.[78] Following this observation, we have selected a constant laser line passage velocity of 0.32 mm s^{-1} to test the influence of thermal fields on BCP ordering in this study. This relatively fast velocity helps mitigate thermal damage to the samples caused by a prolonged residence of BCPs in the hot zone. The results of annealing at faster sweep velocities are presented in SI Figure S12.

Figure 3 shows the influence of the number of annealing cycles and the ambient temperature (T_b, base temperature of the thermal profile) on the quality of alignment of C116 morphology. We quantitatively assessed the degree of alignment by analyzing azimuthal spread of fast Fourier transform (FFT) spectra shown in the insets of SEM images expressed as a circularly wrapped orientational order function:[92,93]

$$I(\varphi) = \frac{1 - \eta^2}{1 + \eta^2 - 4\eta^2 \cos^2 \varphi}$$

where η is the orientational order parameter and φ is the angle along the arc of the FFT image. Interestingly, a significant improvement in the quality of alignment compared with experiments performed at maximum laser power can be attained after lowering it to 24 W and compensating it with increased base temperature (T_b) without encountering a problem of thermal damage to the sample observed at the maximum power (SI Figure S17). To investigate this effect, we selected three different base temperatures, 30, 60, and 90 °C. We intentionally selected the maximum T_b value not to exceed the T_g of both blocks ($\approx$ 100 °C) to limit the isotropic BCP

https://dx.doi.org/10.1021/acsnano.0c00696
ACS Nano 2020, 14, 4805−4815

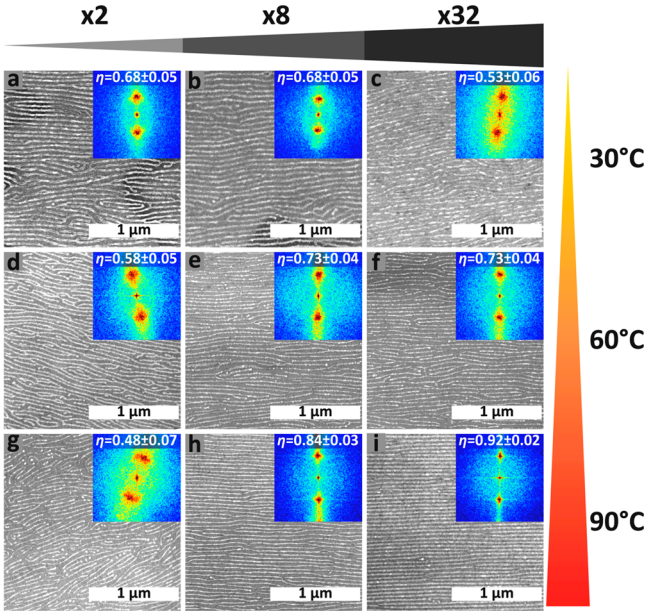

Figure 3. Influence of base temperature and the number of soft-shear laser annealing cycles on PS-*b*-P2VP C116 morphology. SEM images show metallic Pt replicas of the BCP after LA experiment at 24 W and 0.32 mm s^{-1} laser sweeping speed at the base temperature of 30 °C (a–c), 60 °C (d–f), and 90 °C (g–i). The insets show FFTs with calculated orientational order parameter (η) values.

ordering in the regions located on the shoulders of the laser-heated zone. Furthermore, we tested the influence of the annealing time (number of cycles) on the degree of alignment. Even at the lowest base temperature, just 2 cycles of annealing, lasting only 2 min, are sufficient to order the BCP and orient its morphology (Figure 3a). Nevertheless, the decrease in laser power results in the proportional down-shift of the thermal profile, and only a moderate degree of morphology alignment is observed, as shown in Figure 3a–c. For the increased base temperature series (60 °C), we observed a moderate improvement in η but a lack of clear progression of this parameter with time (Figures 3d,e). Increasing the T_b even further, to 90 °C, radically improves the quality of alignment. After 32 cycles of processing (Figure 3i), η reaches a near-saturation value, and its deviation from unity results from the initial choice of the analysis parameters (background cutoff value in FFTs) which are set for all analyzed images. We postulate that this effect results from the widening of the hot zone in which the BCP resides and in which its morphology can respond by aligning to relieve the accumulated stress field induced by expansion of the PDMS. Importantly, the zone has to be hot enough to enable such morphological rearrangement, thus the observed increase in order parameter with the number of annealing cycles.

Extending the width of the heated zone and increasing the corresponding residence time in the hot zone has a negative impact on polymer thermal stability. Block copolymer morphologies have been shown to survive exposure to surprisingly high temperatures provided that the residence time at elevated temperatures is adequately short.[24,75,94] To test the threshold of thermal damage of laser-heated PS-*b*-P2VP BCPs in vacuum, we performed a series of high-power (27 W), high base temperature annealing experiments. We identified the cumulative residence time of approximately 10 s at 300 °C (arbitrary reference temperature) to be the safe limit for thermal damage, as seen in the sample processed at T_b = 60 °C for 8 cycles at 0.32 mm s^{-1}, which does not present signs of thermal degradation (Figure 4a). Conversely, an increase of

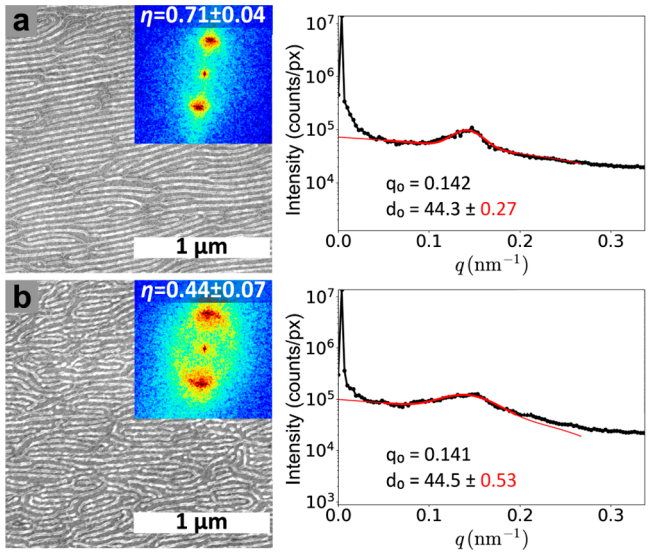

Figure 4. SEM morphologies of C116 PS-*b*-P2VP after ordering at the maximum laser power (27 W) with corresponding FFT circular average plots. (a) After 8 cycles of laser passage at a base temperature of 60 °C and (b) displaying symptoms of thermal degradation after 32 cycles at 90 °C. Laser line velocity was 0.32 mm s^{-1}. The images show a metalized (Pt) replica of the minority P2VP domains. The insets show FFTs with calculated orientational order parameter (η) values. In circularly averaged plots q_0 indicates the primary peak position in the FFT and d_0 is a corresponding real-space periodicity.

base temperature to 90 °C, which increases the residence time at 300 °C to 25 s, leads to thermal damage at the same processing conditions. Even though the macroscopic symptoms of thermal degradation and dewetting were still not observed, the quality of alignment quantitatively measured by the azimuthal spread of the FFT of the SEM image indicates a large spread in the in-plane orientation of the domains. Moreover, we observed an increased deviation in the cylinder-to-cylinder distance manifested by the widening of the FFT correlation peak in the radial direction (Figure 4b). We attribute this effect to partial degradation of BCP and chain fragmentation, which increase the polydispersity index of polymer chains.[15]

Furthermore, at high-power processing conditions, we periodically encountered a problem of uncontrolled PDMS delamination from the BCP surface during the soft-shearing experiments, leading to instantaneous degradation and ashing of the elastomer (SI Figure S17). We observed that such incidents are usually triggered by the hot-spots located near the air pockets entrapped near the solid particulates at the boundary between PDMS and BCP. To reduce this type of surface contaminants, we microfiltered BCP solutions prior to deposition on Si and removed air bubbles trapped under PDMS by an application of vacuum.

We tested the utility of soft-shear laser annealing in alignment of homologous PS-*b*-P2VP cylindrical diblock copolymers of various molecular weights, starting from 45 kg/mol (C45), to relatively large molecular weight, 188 kg/

https://dx.doi.org/10.1021/acsnano.0c00696
ACS Nano 2020, 14, 4805–4815

mol (C188) and 275 kg/mol (C275), materials. Under the LA processing conditions optimized for annealing (P = 24 W, T_b = 90 °C, v = 0.32 mm s^{-1}) and after 8 cycles, the ordering and alignment were observed in all tested systems as shown in Figure 5a. Although the dislocation defects in the BCP

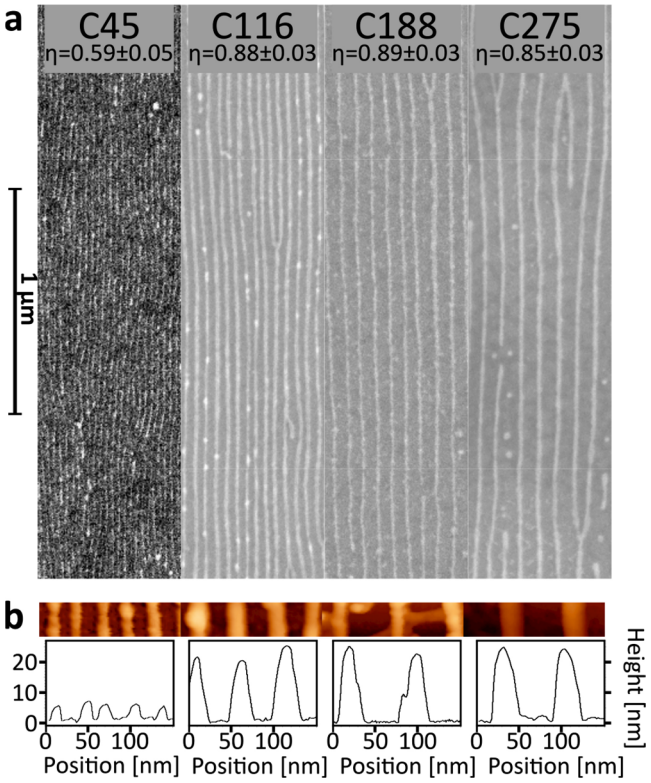

Figure 5. Platinum nanowires templated from laser-aligned cylinder-forming PS-*b*-P2VP homologues of different molecular weight obtained by the optimized SS-LZA procedure (24 W, 90 °C base temperature, 8 cycles at 0.32 mm s^{-1}). (a) Orientational order parameters η that were calculated from FFTs of SEM images indicate high quality of BCP morphology alignment. (b) AFM height images and their cross sections reveal the topography of the wires replicating the cylindrical shape of the poly(2-vinylpyridine) cylindrical domains.

morphologies were not completely eliminated, we have observed that we can minimize their density by optimizing the thickness of the film. We found the optimum value to be ~20% greater than the BCP periodicity (L_0). The periodicity values inferred from analysis of SEM or AFM images analysis (Figure 5b and c) equal 30, 45, 70, and 82 nm for C45, C116, C188, and C275, respectively. The panels in Figure 5b represented cross sections of AFM images perpendicular to the orientation of the BCP nanowire replica, revealing their three-dimensional cylindrical shape. The difference in height between C45 and C116 is quite significant, around 15 nm. On the other hand, heights of C116, C188, and C275 are similar (21−24 nm). It is likely that the AFM tip was not able to scan deep enough to probe the absolute height value.

The fact that high-molecular-weight BCPs, *e.g.*, C275, are alignable using our laser annealing method underlines the utility of this technique for processing large-MW BCPs for which the microphase separation and kinetics of the grain-growth process rapidly decrease with the polymer's degree of polymerization.[95] Moreover, C116, C188, and C275 PS-*b*-P2VP homologues do not form well-ordered horizontal cylinder morphologies during conventional thermal annealing. Instead, they self-assemble into poorly ordered vertical cylinders (SI Figure S18), which indicates the importance of the soft-shearing component.

ALIGNED BCP AS SYNTHETIC TEMPLATES FOR MULTILAYERED NANOMATERIALS

We used block copolymer films aligned in our laser-annealing apparatus as selective deposition templates for patterning inorganic nanomaterials on various substrates. Block copolymers containing 2-vinylpyridine blocks can be readily converted to a metal or a metal oxide replica in processes known as aqueous metal reduction (AMR)[91] or sequential infiltration synthesis (SIS),[96] respectively. Here, we take advantage of the high-throughput capability of our laser annealer, which allows preparation of large-area aligned BCP films on Si substrates, which are subsequently used as patterning templates. As demonstrated herein, the aligned master templates can be floated onto a water surface and easily transferred onto new substrates (Figure 6a). The flotation and

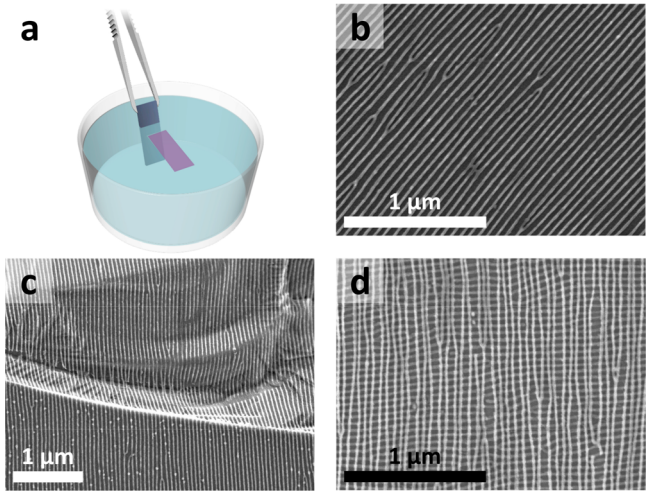

Figure 6. Wet transfer technique of patterning surfaces with laser-aligned C116 PS-*b*-P2VP BCP films. The flotation of the aligned film on the water surface after dissolution of the poly(4-styrene sodium sulfonate) sacrificial layer (a). The aligned film retains the high quality of morphological alignment after it is collected on a fresh Si wafer and metalized to produce an array of Pt nanowires (b). The wires conformally coat a sharp step near the edge of the wafer (c). Two-layer rectangular Pt nanomesh obtained after single-step metalization performed after stacking the aligned BCP films (d).

transfer steps rely on the use of water-soluble sacrificial polymer[64] or acid-soluble oxide layer[97] underlying the BCP film. After performing several experiments with various sacrificial-layer materials, poly(acrylic acid) (PAA), poly(diallyldimethylammonium chloride) (PDADMAC), and polystyrene sodium sulfonate (PSSS), we concluded that only PSSS is fully compatible with our laser annealing process and, unlike PAA, it does not develop cracks even under extreme heating conditions. Moreover, as opposed to acidic PAA and PDADMAC, it does not have a tendency to form the ionic or hydrogen-bonded complexes with the vinylpyridine residues in PS-*b*-P2VP. After rapid dissolution of a 500 nm thick sacrificial PSSS layer and flotation on the water surface,

https://dx.doi.org/10.1021/acsnano.0c00696
ACS Nano 2020, 14, 4805−4815

the aligned BCP films can be readily transferred onto a new substrate without compromising the quality of alignment. Figure 6a shows the Pt replica of the C116 film aligned by the optimized SS-LZA protocol after the transfer onto another Si wafer. The BCP conformally adheres to the new substrate during gentle air drying followed by metalization and plasma removal of the organic template. An array of Pt nanowires oriented perpendicularly to the diced edge continuously coats a deep (~2 μm) vertical step and its edges without visible wrinkles, providing a clear evidence of the conformality of the coating. To demonstrate that, we have transferred the aligned S2VP C116 layer onto an edge of a diced silicon wafer.

As demonstrated previously, BCP-derived nanostructures can be assembled in a step-by-step fashion, leading to multilayered structures of interesting architectures and functionalities.[79,98−103] Unfortunately, this step-by-step approach in which each deposited layer is individually annealed (or aligned) is rather laborious and time-consuming. Our approach to multilayered BCP-derived nanoarchitectures consists in stacking multiple layers of prealigned BCP film, *i.e.*, pieces of the large-area template with a control of registry of alignment between the layers. After the stacking and drying, the layers are converted to the inorganic nanomesh replica in a single conversion step. We show the utility of this approach by assembling a double-layered rectangular *nanonet* (Figure 6d) composed of two orthogonally crossed arrays of Pt nanowires derived from a stack of two C116 layers metalized by a single exposure to a platinum salt solution. The quality of the NW array of the top layer slightly deteriorates compared with the bottom one, as evidenced by the broadening of the FFT resulting from the lateral shifting of the NWs from the former P2VP cylinders' equilibrium positions. On closer inspection, we ascribe these shifts to the lateral movements of the NWs during the plasma etching, rather than to deformations in the BCP film during the transfer, since the latter were not observed during the monolayer transfers. It is likely that the top-layer NWs displace when the oxygen plasma is undercutting the polystyrene layer by which they are supported. The exposed NWs tend to be attracted to their nearest neighbors due to the preferential interaction energy between the freshly formed metallic surfaces.

We tested the robustness of our patterning method by transferring the aligned BCP films onto colloidal silica particles (~800 nm in diameter) sparsely deposited on a Si surface. Electron microscopy images of the silica spheres trapped under the Pt nanonets are presented in Figure 7a−c. Interestingly, the nets adhere tightly to the top half of the spheres and detach from the curved surface near the equator, reminiscent of a drop-cloth draping. The free-standing part of the net forms a ~30° angle with the Si surface and a 35° angle with the sphere, relative to the normal surface vector at the point of contact.

CONCLUSIONS

In conclusion, we have demonstrated a facile way of obtaining large-area uniaxially aligned cylindrical PS-*b*-P2VP BCP films on easily accessible silicon substrates by cold-zone (*i.e.*, without crossing the T_{ODT}) laser annealing coupled to soft shearing. Our method utilizes an industrial-grade diode laser, which is an economical alternative to research-grade laser sources. The diode radiation is coupled to an optical fiber and delivered to a lightweight processing head, which renders the annealing setup extremely compact. We believe that these features of our setup facilitate broader utilization and development of the laser annealing technique.

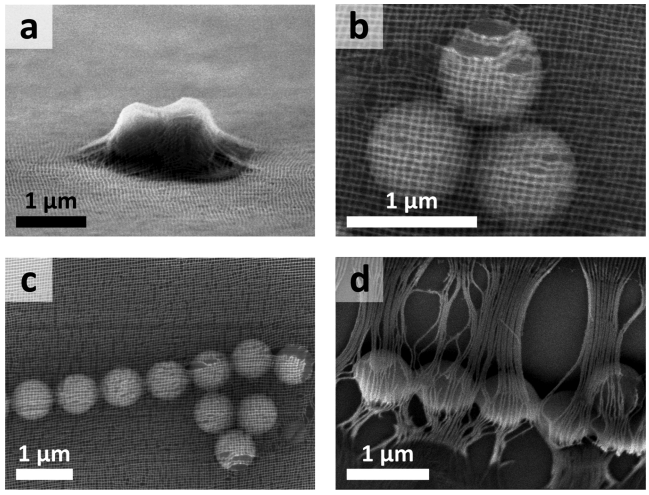

Figure 7. Patterning high-curvature 3D objects with nanonets made from two layers of block copolymer. Side-view (a) and top-down (b and c) SEM images of 800 nm silica spheres draped with platinum nanonets obtained by metalization of two layers of aligned cylindrical C116 PS-*b*-P2VP crossed at ~90°. Mechanically, the crossed meshes are more stable than single-layer arrays, which do not withstand plasma-ashing removal of the BCP template and tend to form bundles in the unsupported regions (d).

We have also demonstrated that all steps of laser annealing can be successfully performed on BCP films coated on top of a water-soluble sodium poly(styrenesulfonate) sacrificial layer allowing transfer of the aligned BCP films onto arbitrary substrates. A key advantage of the presented fabrication approach is the acceleration of the previously described step-by-step laser-assisted fabrication of multilayered BCP architectures.[79,102] In principle, only a single laser-annealing step is needed to prepare a reservoir (*e.g.*, long sheet or roll) of well-aligned BCP film, which can be readily transferred and stacked on a new substrate. Interestingly, this wet transfer approach yields conformal coating of highly corrugated substrates.

METHODS

Materials. Standard ~500 μm thick single-sided polished electronic-grade boron-doped ⟨100⟩ Si wafers purchased from ITME, Poland, were used as polymer substrates. Cylinder-forming polystyrene-*block*-poly(2-vinylpyridine) (PS-*b*-P2VP) with PS majority block and the composition 33.3 kg/mol-*b*-11.0 kg/mol (PDI = 1.05), 79.0 kg/mol-*b*-36.5 kg/mol (PDI = 1.05), 135 kg/mol-*b*-53 kg/mol (PDI = 1.18), 185 kg/mol-*b*-90 kg/mol (PDI = 1.10) were obtained from Polymer Source. In correspondence to the their cylindrical morphology and total molecular weight, they are abbreviated as C45, C116, C188, and C275, respectively.

Thin Film Casting. The polymers were dissolved in dry toluene (GPC grade, Carl Roth) to yield 1% (C45) and 1.5% (C116, C188, C275) w/w solutions. Solutions were filtered with a 0.20 μm PTFE syringe filter. Silicon substrates (12 mm × 12 mm) were briefly cleaned with oxygen plasma (PE-25, Plasma Etch, 150 mTorr O_2, 100 W RF power, 120 s) immediately before the spin coating (SPIN150i, SPS-Europe). Spin-coating speeds were adjusted to target dry-state film thicknesses corresponding to approximately 1.2 cylinder-to-cylinder distance (L_0) in each BCP, e.g., 60 nm obtained at 2000 rpm for 60 s in the case of C116 PS-*b*-P2VP for which L_0 = 45 nm. Film thicknesses were measured using an optical reflectometer (F-20, Filmetrics).

https://dx.doi.org/10.1021/acsnano.0c00696
ACS Nano 2020, 14, 4805−4815

Laser Annealing Setup. A high-power (30 W) solid-state 980 nm near-IR fiber diode laser supplied by Tomorrow's System Ltd. was used in photothermal annealing experiments. The beam emitted by the fiber (NA = 0.22) was first collimated and then focused by a pair of AR-coated plano-convex spherical and cylindrical lenses to project a narrow line (120 μm fwhm by approximately 7 mm) onto the horizontal plane of the substrate. The focus position was adjusted with a micrometer-screw-driven translation of the optics pair, which allowed compensation of the focus-plane shift due to the presence of the vacuum window or controlled deliberate defocusing. Optical profiles of the laser line were recorded by a CMOS beam profiler (CinCam CMOS-1201-Nano, CINOGY) with a sensor positioned in the sample plane. Laser power calibration was performed with a thermal power sensor (PM310D, Thorlabs) positioned behind the vacuum chamber window to accurately measure light intensity arriving at the sample. Far field surface temperature profiles were acquired under laser irradiation using a temperature logger with a fine-gauge thermocouple sensor (K-type, 50 μm diameter, Omega Engineering Inc.) secured at the center of the Si test chip surface with a small amount of high-temperature cement (Omega Engineering Inc.). The test chip was mounted on the XY-translation stage in place of a regular sample and scanned in 100 μm steps in the direction perpendicular to the laser line to obtain the transverse temperature profile of the hot zone. The scans were repeated at different positions along the laser line. In the optical configuration used in this study, at the illumination power of 27 W the width of the thermal profile was 1020 μm (fwhm) with the maximum temperature reaching 310 °C. Length-wise thermal profiling revealed that the temperatures are highly uniform within the central portion of the line and drop by 10 °C from the maximum temperature 3 mm away from the center. The setup is equipped with electrical resistive heaters to provide an additional degree of control over the base processing temperature (T_b) of the chamber and fan cooling to help stabilize the temperature by dissipating the heat delivered by the laser beam.

Laser Annealing with Soft Shearing. Si substrates with BCP films were mounted on the polished surface of the aluminum baseplate after application of a thin layer (50 μm) of nonvolatile silicone grease (Dow Corning, high-vacuum silicone grease). The use of grease, which provides thermal contact between the silicon and the baseplate, is critical to prevent thermal runaways during laser annealing in vacuum. Polydimethylsiloxane pads of 700 μm thick (PDMS, Dow Corning, Sylgard 184, 5:1 ratio of resin-to-cross-linker) were prepared by curing a deaerated mixture under mild vacuum (0.1 bar) at 80 °C for 24 h. The pads were cut to wafer size and gently transferred onto the top surface of the polymer films. The carrier bar supporting the samples was placed inside a thermostated vacuum chamber (≈ 1.0 mbar) fitted with a transparent glass window attached to a motorized motion stage (ILS 250CC, Newport). The base temperature of the chamber was stabilized for 15 min before starting the laser heating. During laser annealing experiments, a constant laser power of 24 W was used. The samples were swept across the laser line at the constant velocity 0.32 mm s^{-1}, previously optimized in terms of the alignment response of PS-*b*-P2VP to photothermal shearing.[78] If multiple sweeps were performed, the stage was moved across the beam in both directions in a cyclic manner. PDMS pads were peeled off from BCP samples immediately after the annealing was completed.

Transferrable Polymer Film Preparation. A 15% w/w solution of poly(4-styrene sodium sulfonate) was obtained by diluting the commercial 30% solution (70 kg/mol Sigma-Aldrich) with DI water. Silicon substrates were coated with a 500 nm thick water-soluble sacrificial layer of PSSS by spin-casting at 2000 rpm for 60 s followed by air-drying on a hot plate at 100 °C for 300 s. BCP films were spin-cast onto PSSS-coated Si substrates immediately after cooling them to room temperature in a stream of dry nitrogen. The coating and laser annealing followed the same protocol as in the case of regular Si substrates. The aligned BCP film transfers were performed after dissolution of the sacrificial PSSS layer and floatation of the films on the surface of DI water. To keep track of the alignment direction, the films on Si were scribed with a rectangular pattern with a tip of a hypodermic needle. The substrates were slowly immersed in water at a 45° angle to avoid mechanical damage of the BCP layer. Progressive dissolving and immersion was continued until only one edge remained attached to the substrate and the floating thin film could be easily picked up by the new substrate. This allowed control of the domain alignment direction, particularly important in the case of the double-layered BCP stacks.

Conversion of BCP Films to Metallic Replicas. P2VP domains in PS-*b*-P2VP block copolymers were selectively coordinated with Pt complex salt by immersion in 20 mM K_2PtCl_4 in 0.5 M HCl for 45 min at room temperature and converted to Pt metallic replicas by plasma etching (120 mTorr O_2, 120 W RF power for 300 s, 35 kHz, plasma etcher PE-25, Plasma Etch) following the protocol described by Buriak and Aizawa.[85] For the double-layered BCP stacks, it is not necessary to metalize each layer separately; two stacked layers of aligned BCPs were complexed and metalized during a single exposure to Pt salt under the same experimental conditions, except for the longer etching time in oxygen plasma equal to 600 s.

Electron Microscopy and Image Analysis Routines. Following the conversion to metallic replicas, the samples were imaged under scanning electron microscopes (FE-SEMs Zeiss Merlin and Hitachi S-4800) operating at 2 keV utilizing an in-lens detector of secondary electrons. FFT analysis and quantification of the degree of alignment in BCP morphologies were performed utilizing Python-written routines from the SciAnalysis package developed by Dr. K. Yager.[104]

Atomic Force Microscopy. AFM measurements were performed using a Dimension Icon instrument (Bruker, USA) in PeakForce tapping mode utilizing ScanAsyst-Air cantilevers with 70 kHz resonant frequency (k = 0.4 N m^{-1}). Height images (2 μm × 2 μm) of metalized samples were obtained in 512 × 512 pixel resolution at 1 Hz line scan rate. The 3D surface visualization images were rendered using Gwyddion software.[105]

ASSOCIATED CONTENT

Supporting Information

The Supporting Information is available free of charge at https://pubs.acs.org/doi/10.1021/acsnano.0c00696.

Detailed description of experimental setup, beam profiling, and surface temperature measurements, numerical simulations of laser heating; additional SEM and AFM images of laser-processed, oven-annealed, and thermally degraded samples (PDF)

AUTHOR INFORMATION

Corresponding Author

Pawel W. Majewski − *Department of Chemistry, University of Warsaw, Warsaw 02089, Poland;* orcid.org/0000-0001-6338-2411; Email: pmajewski@chem.uw.edu.pl

Authors

Arkadiusz A. Leniart − *Department of Chemistry, University of Warsaw, Warsaw 02089, Poland*

Przemyslaw Pula − *Department of Chemistry, University of Warsaw, Warsaw 02089, Poland*

Andrzej Sitkiewicz − *Department of Chemistry, University of Warsaw, Warsaw 02089, Poland*

Complete contact information is available at: https://pubs.acs.org/10.1021/acsnano.0c00696

Notes

The authors declare no competing financial interest.

ACKNOWLEDGMENTS

All authors would like to gratefully acknowledge financial support from the First Team program (POIR.04.04.00-00-1DE6/16) of the Foundation for Polish Science cofinanced by

the European Union under the European Regional Development Fund. P.W.M. also thanks the National Science Center (Poland) for financial support under Grant No. 2015/19/P/ST5/03813, which received funding from the European Union's Horizon 2020 Research and Innovation Program under the Marie Sklodowska-Curie grant agreement No. 665778. This research used resources of the Center for Functional Nanomaterials, which is a U.S. DOE Office of Science Facility, at Brookhaven National Laboratory, under Contract No. DE-SC0012704.

REFERENCES

(1) Bates, C. M.; Bates, F. S. 50th Anniversary Perspective: Block Polymers-Pure Potential. *Macromolecules* **2017**, *50*, 3−22.
(2) Wang, W.; Lu, W.; Kang, N.-G.; Mays, J.; Hong, K. Thermoplastic Elastomers Based on Block, Graft, and Star Copolymers. In *Elastomers*; InTech: London, 2017; pp 97−110.
(3) Agrahari, V.; Agrahari, V. Advances and Applications of Block-Copolymer-Based Nanoformulations. *Drug Discovery Today* **2018**, *23*, 1139−1151.
(4) Hamley, I. W. Ordering in Thin Films of Block Copolymers: Fundamentals to Potential Applications. *Prog. Polym. Sci.* **2009**, *34*, 1161−1210.
(5) Kim, H. C.; Park, S. M.; Hinsberg, W. D.; Division, I. R. Block Copolymer Based Nanostructures: Materials, Processes, and Applications to Electronics. *Chem. Rev.* **2010**, *110*, 146−177.
(6) Yoo, H. G.; Byun, M.; Jeong, C. K.; Lee, K. J. Performance Enhancement of Electronic and Energy Devices *via* Block Copolymer Self-Assembly. *Adv. Mater.* **2015**, *27*, 3982−3998.
(7) Kim, J. H.; Jin, H. M.; Yang, G. G.; Han, K. H.; Yun, T.; Shin, J. Y.; Jeong, S.-J.; Kim, S. O. Smart Nanostructured Materials Based on Self-Assembly of Block Copolymers. *Adv. Funct. Mater.* **2020**, *30*, 1902049.
(8) Jackson, E. A.; Hillmyer, M. A. Nanoporous Membranes Derived from Block Copolymers: From Drug Delivery to Water Filtration. *ACS Nano* **2010**, *4*, 3548−3553.
(9) Abetz, V. Isoporous Block Copolymer Membranes. *Macromol. Rapid Commun.* **2015**, *36*, 10−22.
(10) Nunes, S. P. Block Copolymer Membranes for Aqueous Solution Applications. *Macromolecules* **2016**, *49*, 2905−2916.
(11) Young, W. S.; Kuan, W. F.; Epps, T. H. Block Copolymer Electrolytes for Rechargeable Lithium Batteries. *J. Polym. Sci., Part B: Polym. Phys.* **2014**, *52*, 1−16.
(12) Rojas, A. A.; Inceoglu, S.; Mackay, N. G.; Thelen, J. L.; Devaux, D.; Stone, G. M.; Balsara, N. P. Effect of Lithium-Ion Concentration on Morphology and Ion Transport in Single-Ion-Conducting Block Copolymer Electrolytes. *Macromolecules* **2015**, *48*, 6589−6595.
(13) Phan, T. N. T.; Issa, S.; Gigmes, D. Poly(Ethylene Oxide)-Based Block Copolymer Electrolytes for Lithium Metal Batteries. *Polym. Int.* **2019**, *68*, 7−13.
(14) Bates, C. M.; Maher, M. J.; Janes, D. W.; Ellison, C. J.; Willson, C. G. Block Copolymer Lithography. *Macromolecules* **2014**, *47*, 2−12.
(15) Ferrarese Lupi, F.; Giammaria, T. J.; Seguini, G.; Vita, F.; Francescangeli, O.; Sparnacci, K.; Antonioli, D.; Gianotti, V.; Laus, M.; Perego, M. Fine Tuning of Lithographic Masks through Thin Films of PS-b-PMMA with Different Molar Mass by Rapid Thermal Processing. *ACS Appl. Mater. Interfaces* **2014**, *6*, 7180−7188.
(16) Jeong, S.-J.; Kim, J. Y.; Kim, B. H.; Moon, H.-S.; Kim, S. O. Directed Self-Assembly of Block Copolymers for Next Generation Nanolithography. *Mater. Today* **2013**, *16*, 468−476.
(17) Liapis, A. C.; Rahman, A.; Black, C. T. Self-Assembled Nanotextures Impart Broadband Transparency to Glass Windows and Solar Cell Encapsulants. *Appl. Phys. Lett.* **2017**, *111*, 183901.
(18) Brassat, K.; Kool, D.; Lindner, J. K. N. Modification of Block Copolymer Lithography Masks by O_2/Ar Plasma Treatment: Insights from Lift-Off Experiments, Nanopore Etching and Free Membranes. *Nanotechnology* **2019**, *30*, 225302.
(19) Robb, M. J.; Ku, S. Y.; Hawker, C. J. 25th Anniversary Article: No Assembly Required: Recent Advances in Fully Conjugated Block Copolymers. *Adv. Mater.* **2013**, *25*, 5686−5700.
(20) Lee, Y.; Gomez, E. D. Challenges and Opportunities in the Development of Conjugated Block Copolymers for Photovoltaics. *Macromolecules* **2015**, *48*, 7385−7395.
(21) Mitchell, V. D.; Jones, D. J. Advances toward the Effective Use of Block Copolymers as Organic Photovoltaic Active Layers. *Polym. Chem.* **2018**, *9*, 795−814.
(22) Nagpal, U.; Müller, M.; Nealey, P. F.; De Pablo, J. J. Free Energy of Defects in Ordered Assemblies of Block Copolymer Domains. *ACS Macro Lett.* **2012**, *1*, 418−422.
(23) Li, W.; Müller, M. Defects in the Self-Assembly of Block Copolymers and Their Relevance for Directed Self-Assembly. *Annu. Rev. Chem. Biomol. Eng.* **2015**, *6*, 187−216.
(24) Majewski, P. W.; Yager, K. G. Millisecond Ordering of Block Copolymer Films *via* Photothermal Gradients. *ACS Nano* **2015**, *9*, 3896−3906.
(25) Majewski, P. W.; Yager, K. G. Rapid Ordering of Block Copolymer Thin Films. *J. Phys.: Condens. Matter* **2016**, *28*, 403002.
(26) Hu, H.; Gopinadhan, M.; Osuji, C. O. Directed Self-Assembly of Block Copolymers: A Tutorial Review of Strategies for Enabling Nanotechnology with Soft Matter. *Soft Matter* **2014**, *10*, 3867−3889.
(27) Darling, S. B. Directing the Self-Assembly of Block Copolymers. *Prog. Polym. Sci.* **2007**, *32*, 1152−1204.
(28) Li, W.; Müller, M. Directed Self-Assembly of Block Copolymers by Chemical or Topographical Guiding Patterns: Optimizing Molecular Architecture, Thin-Film Properties, and Kinetics. *Prog. Polym. Sci.* **2016**, *54*, 47−75.
(29) Pereira, G. G.; Williams, D. R. M. Diblock Copolymer Melts in Electric Fields: The Transition from Parallel to Perpendicular Alignment Using a Capacitor Analogy. *Macromolecules* **1999**, *32*, 8115−8120.
(30) Xu, T.; Zvelindovsky, A. V.; Sevink, G. J. A.; Lyakhova, K. S.; Jinnai, H.; Russell, T. P. Electric Field Alignment of Asymmetric Diblock Copolymer Thin Films. *Macromolecules* **2005**, *38*, 10788−10798.
(31) Liedel, C.; Pester, C. W.; Ruppel, M.; Urban, V. S.; Böker, A. Beyond Orientation: The Impact of Electric Fields on Block Copolymers. *Macromol. Chem. Phys.* **2012**, *213*, 259−269.
(32) Jeon, H. U.; Jin, H. M.; Kim, J. Y.; Cha, S. K.; Mun, J. H.; Lee, K. E.; Oh, J. J.; Yun, T.; Kim, J. S.; Kim, S. O. Electric Field Directed Self-Assembly of Block Copolymers for Rapid Formation of Large-Area Complex Nanopatterns. *Mol. Syst. Des. Eng.* **2017**, *2*, 560−566.
(33) Park, M. J.; Balsara, N. P. Anisotropic Proton Conduction in Aligned Block Copolymer Electrolyte Membranes at Equilibrium with Humid Air. *Macromolecules* **2010**, *43*, 292−298.
(34) McCulloch, B.; Portale, G.; Bras, W.; Pople, J. A.; Hexemer, A.; Segalman, R. A. Dynamics of Magnetic Alignment in Rod-Coil Block Copolymers. *Macromolecules* **2013**, *46*, 4462−4471.
(35) Majewski, P. W.; Gopinadhan, M.; Osuji, C. O. Magnetic Field Alignment of Block Copolymers and Polymer Nanocomposites: Scalable Microstructure Control in Functional Soft Materials. *J. Polym. Sci., Part B: Polym. Phys.* **2012**, *50*, 2−8.
(36) Rokhlenko, Y.; Majewski, P. W.; Larson, S. R.; Gopalan, P.; Yager, K. G.; Osuji, C. O. Implications of Grain Size Variation in Magnetic Field Alignment of Block Copolymer Blends. *ACS Macro Lett.* **2017**, *6*, 404−409.
(37) Majewski, P. W.; Gopinadhan, M.; Osuji, C. O. The Effects of Magnetic Field Alignment on Lithium Ion Transport in a Polymer Electrolyte Membrane with Lamellar Morphology. *Polymers* **2019**, *11*, 887.
(38) Angelescu, D. E.; Waller, J. H.; Adamson, D. H.; Deshpande, P.; Chou, S. Y.; Register, R. A.; Chaikin, P. M. Macroscopic Orientation of Block Copolymer Cylinders in Single-Layer Films by Shearing. *Adv. Mater.* **2004**, *16*, 1736−1740.
(39) Davis, R. L.; Chaikin, P. M.; Register, R. A. Cylinder Orientation and Shear Alignment in Thin Films of Polystyrene-

https://dx.doi.org/10.1021/acsnano.0c00696
ACS Nano 2020, 14, 4805−4815

Poly(n-Hexyl Methacrylate) Diblock Copolymers. *Macromolecules* **2014**, *47*, 5277−5285.
(40) Sundrani, D.; Darling, S. B.; Sibener, S. J. Guiding Polymers to Perfection: Macroscopic Alignment of Nanoscale Domains. *Nano Lett.* **2004**, *4*, 273−276.
(41) Bita, I.; Yang, J. K. W.; Yeon, S. J.; Ross, C. A.; Thomas, E. L.; Berggren, K. K. Graphoepitaxy of Self-Assembled Block Copolymers on Two-Dimensional Periodic Patterned Templates. *Science* **2008**, *321*, 939−943.
(42) Hong, S. W.; Huh, J.; Gu, X.; Lee, D. H.; Jo, W. H.; Park, S.; Xu, T.; Russell, T. P. Unidirectionally Aligned Line Patterns Driven by Entropic Effects on Faceted Surfaces. *Proc. Natl. Acad. Sci. U. S. A.* **2012**, *109*, 1402−1406.
(43) Brassat, K.; Kool, D.; Nallet, C. G. A.; Lindner, J. K. N. Understanding Film Thickness-Dependent Block Copolymer Self-Assembly by Controlled Polymer Dewetting on Prepatterned Surfaces. *Adv. Mater. Interfaces* **2020**, *7*, 1901605.
(44) Lee, D. E.; Ryu, J.; Hong, D.; Park, S.; Lee, D. H.; Russell, T. P. Directed Self-Assembly of Asymmetric Block Copolymers in Thin Films Driven by Uniaxially Aligned Topographic Patterns. *ACS Nano* **2018**, *12*, 1642−1649.
(45) Kim, S. O.; Solak, H. H.; Stoykovich, M. P.; Ferrier, N. J.; De Pablo, J. J.; Nealey, P. F. Epitaxial Self-Assembly of Block Copolymers on Lithographically Defined Nanopatterned Substrates. *Nature* **2003**, *424*, 411−414.
(46) Ruiz, R.; Kang, H.; Detcheverry, F. A.; Dobisz, E.; Kercher, D. S.; Albrecht, T. R.; De Pablo, J. J.; Nealey, P. F. Density Multiplication and Improved Lithography by Directed Block Copolymer Assembly. *Science* **2008**, *321*, 936−939.
(47) Williamson, L. D.; Seidel, R. N.; Chen, X.; Suh, H. S.; Rincon Delgadillo, P.; Gronheid, R.; Nealey, P. F. Three-Tone Chemical Patterns for Block Copolymer Directed Self-Assembly. *ACS Appl. Mater. Interfaces* **2016**, *8*, 2704−2712.
(48) Doerk, G. S.; Yager, K. G. Rapid Ordering in "Wet Brush" Block Copolymer/Homopolymer Ternary Blends. *ACS Nano* **2017**, *11*, 12326−12336.
(49) Albert, J. N. L.; Bogart, T. D.; Lewis, R. L.; Beers, K. L.; Fasolka, M. J.; Hutchison, J. B.; Vogt, B. D.; Epps, T. H. Gradient Solvent Vapor Annealing of Block Copolymer Thin Films Using a Microfluidic Mixing Device. *Nano Lett.* **2011**, *11*, 1351−1357.
(50) Sinturel, C.; Vayer, M.; Morris, M.; Hillmyer, M. A. Solvent Vapor Annealing of Block Polymer Thin Films. *Macromolecules* **2013**, *46*, 5399−5415.
(51) Gotrik, K. W.; Ross, C. A. Solvothermal Annealing of Block Copolymer Thin Films. *Nano Lett.* **2013**, *13*, 5117−5122.
(52) Modi, A.; Bhaway, S. M.; Vogt, B. D.; Douglas, J. F.; Al-Enizi, A.; Elzatahry, A.; Sharma, A.; Karim, A. Direct Immersion Annealing of Thin Block Copolymer Films. *ACS Appl. Mater. Interfaces* **2015**, *7*, 21639−21645.
(53) Park, W. I.; Kim, J. M.; Jeong, J. W.; Jung, Y. S. Deep-Nanoscale Pattern Engineering by Immersion-Induced Self-Assembly. *ACS Nano* **2014**, *8*, 10009−10018.
(54) Berry, B. C.; Bosse, A. W.; Douglas, J. F.; Jones, R. L.; Karim, A. Orientational Order in Block Copolymer Films Zone Annealed below the Order-Disorder Transition Temperature. *Nano Lett.* **2007**, *7*, 2789−2794.
(55) Yager, K. G.; Fredin, N. J.; Zhang, X.; Berry, B. C.; Karim, A.; Jones, R. L. Evolution of Block-Copolymer Order through a Moving Thermal Zone. *Soft Matter* **2010**, *6*, 92−99.
(56) Bodycomb, J.; Funaki, Y.; Kimishima, K.; Hashimoto, T. Single-Grain Lamellar Microdomain from a Diblock Copolymer. *Macromolecules* **1999**, *32*, 2075−2077.
(57) Hashimoto, T.; Bodycomb, J.; Funaki, Y.; Kimishima, K. The Effect of Temperature Gradient on the Microdomain Orientation of Diblock Copolymers Undergoing an Order-Disorder Transition. *Macromolecules* **1999**, *32*, 952−954.
(58) Mita, K.; Tanaka, H.; Saijo, K.; Takenaka, M.; Hashimoto, T. Ordering of Cylindrical Domains of Block Copolymers under Moving Temperature Gradient: Separation of ∇T-Induced Ordering from Surface-Induced Ordering. *Macromolecules* **2008**, *41*, 6787−6792.
(59) Angelescu, D. E.; Waller, J. H.; Adamson, D. H.; Register, R. A.; Chaikin, P. M. Enhanced Order of Block Copolymer Cylinders in Single-Layer Films Using a Sweeping Solidification Front. *Adv. Mater.* **2007**, *19*, 2687−2690.
(60) Lovinger, A. J.; Chua, J. O.; Gryte, C. C. Studies on the α and β Forms of Isotactic Polypropylene by Crystallization in a Temperature Gradient. *J. Polym. Sci., Polym. Phys. Ed.* **1977**, *15*, 641−656.
(61) De Rosa, C.; Park, C.; Thomas, E. L.; Lotz, B. Microdomain Patterns from Directional Eutectic Solidification and Epitaxy. *Nature* **2000**, *405*, 433−437.
(62) Mita, K.; Tanaka, H.; Saijo, K.; Takenaka, M.; Hashimoto, T. Macroscopically Oriented Lamellar Microdomains Created by "Cold Zone-Heating" Method Involving OOT. *Polymer* **2008**, *49*, 5146−5157.
(63) Singh, G.; Yager, K. G.; Smilgies, D. M.; Kulkarni, M. M.; Bucknall, D. G.; Karim, A. Tuning Molecular Relaxation for Vertical Orientation in Cylindrical Block Copolymer Films *via* Sharp Dynamic Zone Annealing. *Macromolecules* **2012**, *45*, 7107−7117.
(64) Singh, G.; Batra, S.; Zhang, R.; Yuan, H.; Yager, K. G.; Cakmak, M.; Berry, B.; Karim, A. Large-Scale Roll-to-Roll Fabrication of Vertically Oriented Block Copolymer Thin Films. *ACS Nano* **2013**, *7*, 5291−5299.
(65) Singh, G.; Yager, K. G.; Berry, B.; Kim, H. C.; Karim, A. Dynamic Thermal Field-Induced Gradient Soft-Shear for Highly Oriented Block Copolymer Thin Films. *ACS Nano* **2012**, *6*, 10335−10342.
(66) Qiang, Z.; Zhang, Y.; Groff, J. A.; Cavicchi, K. A.; Vogt, B. D. A Generalized Method for Alignment of Block Copolymer Films: Solvent Vapor Annealing with Soft Shear. *Soft Matter* **2014**, *10*, 6068−6076.
(67) Luo, M.; Scott, D. M.; Epps, T. H. Writing Highly Ordered Macroscopic Patterns in Cylindrical Block Polymer Thin Films *via* Raster Solvent Vapor Annealing and Soft Shear. *ACS Macro Lett.* **2015**, *4*, 516−520.
(68) Tan, K. W.; Wiesner, U. Block Copolymer Self-Assembly Directed Hierarchically Structured Materials from Nonequilibrium Transient Laser Heating. *Macromolecules* **2019**, *52*, 395−409.
(69) Nowak, S. R.; Yager, K. G. Photothermally Directed Assembly of Block Copolymers. *Adv. Mater. Interfaces* **2020**, *7*, 1901679.
(70) Jacobs, A. G.; Liedel, C.; Peng, H.; Wang, L.; Smilgies, D. M.; Ober, C. K.; Thompson, M. O. Kinetics of Block Copolymer Phase Segregation during Sub-Millisecond Transient Thermal Annealing. *Macromolecules* **2016**, *49*, 6462−6470.
(71) Jiang, J.; Jacobs, A.; Thompson, M. O.; Ober, C. K. Laser Spike Annealing of DSA Photoresists. *J. Photopolym. Sci. Technol.* **2015**, *28*, 631−634.
(72) Yong, D.; Jin, H. M.; Kim, S. O.; Kim, J. U. Laser-Directed Self-Assembly of Highly Aligned Lamellar and Cylindrical Block Copolymer Nanostructures: Experiment and Simulation. *Macromolecules* **2018**, *51*, 1418−1426.
(73) Bell, R. T.; Jacobs, A. G.; Sorg, V. C.; Jung, B.; Hill, M. O.; Treml, B. E.; Thompson, M. O. Lateral Temperature-Gradient Method for High-Throughput Characterization of Material Processing by Millisecond Laser Annealing. *ACS Comb. Sci.* **2016**, *18*, 548−558.
(74) Jiang, J.; Jacobs, A. G.; Wenning, B.; Liedel, C.; Thompson, M. O.; Ober, C. K. Ultrafast Self-Assembly of Sub-10 nm Block Copolymer Nanostructures by Solvent-Free High-Temperature Laser Annealing. *ACS Appl. Mater. Interfaces* **2017**, *9*, 31317−31324.
(75) Jin, H. M.; Lee, S. H.; Kim, J. Y.; Son, S. W.; Kim, B. H.; Lee, H. K.; Mun, J. H.; Cha, S. K.; Kim, J. S.; Nealey, P. F.; Lee, K. J.; Kim, S. O. Laser Writing Block Copolymer Self-Assembly on Graphene Light-Absorbing Layer. *ACS Nano* **2016**, *10*, 3435−3442.
(76) Jin, H. M.; Park, D. Y.; Jeong, S. J.; Lee, G. Y.; Kim, J. Y.; Mun, J. H.; Cha, S. K.; Lim, J.; Kim, J. S.; Kim, K. H.; Lee, K. J.; Kim, S. O. Flash Light Millisecond Self-Assembly of High χ Block Copolymers for Wafer-Scale Sub-10 nm Nanopatterning. *Adv. Mater.* **2017**, *29*, 1700595.

https://dx.doi.org/10.1021/acsnano.0c00696
ACS Nano 2020, 14, 4805−4815

(77) Singer, J. P.; Gotrik, K. W.; Lee, J. H.; Kooi, S. E.; Ross, C. A.; Thomas, E. L. Alignment and Reordering of a Block Copolymer by Solvent-Enhanced Thermal Laser Direct Write. *Polymer* **2014**, *55*, 1875−1882.
(78) Majewski, P. W.; Yager, K. G. Block Copolymer Response to Photothermal Stress Fields. *Macromolecules* **2015**, *48*, 4591−4598.
(79) Majewski, P. W.; Rahman, A.; Black, C. T.; Yager, K. G. Arbitrary Lattice Symmetries *via* Block Copolymer Nanomeshes. *Nat. Commun.* **2015**, *6*, 7448.
(80) Majewski, P. W.; Yager, K. G. Latent Alignment in Pathway-Dependent Ordering of Block Copolymer Thin Films. *Nano Lett.* **2015**, *15*, 5221−5228.
(81) Lide, D. R. *CRC Handbook of Chemistry and Physics*, 84th ed.; 2003−2004, CRC Press: Boca Raton, FL, 2003; pp 12−195.
(82) Singer, J. P.; Lin, P. T.; Kooi, S. E.; Kimerling, L. C.; Michel, J.; Thomas, E. L. Direct-Write Thermocapillary Dewetting of Polymer Thin Films by a Laser-Induced Thermal Gradient. *Adv. Mater.* **2013**, *25*, 6100−6105.
(83) Singer, J. P.; Kooi, S. E.; Thomas, E. L. Focused Laser-Induced Marangoni Dewetting for Patterning Polymer Thin Films. *J. Polym. Sci., Part B: Polym. Phys.* **2016**, *54*, 225−236.
(84) Green, M. A.; Keevers, M. J. Optical Properties of Intrinsic Silicon at 300 K. *Prog. Photovoltaics* **1995**, *3*, 189−192.
(85) Aizawa, M.; Buriak, J. M. Block Copolymer Templated Chemistry for the Formation of Metallic Nanoparticle Arrays on Semiconductor Surfaces. *Chem. Mater.* **2007**, *19*, 5090−5101.
(86) Shin, W. J.; Kim, J. Y.; Cho, G.; Lee, J. S. Highly Selective Incorporation of SiO2 Nanoparticles in PS-b-P2VP Block Copolymers by Quaternization. *J. Mater. Chem.* **2009**, *19*, 7322−7325.
(87) Stankova, N. E.; Atanasov, P. A.; Nikov, R. G.; Nikov, R. G.; Nedyalkov, N. N.; Stoyanchov, T. R.; Fukata, N.; Kolev, K. N.; Valova, E. I.; Georgieva, J. S.; Armyanov, St. A. Optical Properties of Polydimethylsiloxane (PDMS) during Nanosecond Laser Processing. *Appl. Surf. Sci.* **2016**, *374*, 96−103.
(88) Singer, J. P. Thermocapillary Approaches to the Deliberate Patterning of Polymers. *J. Polym. Sci., Part B: Polym. Phys.* **2017**, *55*, 1649−1668.
(89) Okada, Y.; Tokumaru, Y. Precise Determination of Lattice Parameter and Thermal Expansion Coefficient of Silicon between 300 and 1500 K. *J. Appl. Phys.* **1984**, *56*, 314−320.
(90) Mark, J. E. *Polymer Data Handbook*; Oxford University Press: New York, 1999; p 417.
(91) Chai, J.; Buriak, J. M. Using Cylindrical Domains of Block Copolymers to Self-Assemble and Align Metallic Nanowires. *ACS Nano* **2008**, *2*, 489−501.
(92) Ruland, W.; Smarsly, B. SAXS of Self-Assembled Oriented Lamellar Nano-Composite Films: An Advanced Method of Evaluation. *J. Appl. Crystallogr.* **2004**, *37*, 575−584.
(93) Majewski, P. W.; Yager, K. G. Reordering Transitions during Annealing of Block Copolymer Cylinder Phases. *Soft Matter* **2016**, *12*, 281−294.
(94) Tan, K. W.; Jung, B.; Werner, J. G.; Rhoades, E. R.; Thompson, M. O.; Wiesner, U. Transient Laser Heating Induced Hierarchical Porous Structures from Block Copolymer-Directed Self-Assembly. *Science* **2015**, *349*, 54−58.
(95) Seguini, G.; Zanenga, F.; Laus, M.; Perego, M. Ordering Kinetics in Two-Dimensional Hexagonal Pattern of Cylinder-Forming PS-b-PMMA Block Copolymer Thin Films: Dependence on the Segregation Strength. *Phys. Rev. Mater.* **2018**, *2*, 55605.
(96) Peng, Q.; Tseng, Y. C.; Darling, S. B.; Elam, J. W. A Route to Nanoscopic Materials *via* Sequential Infiltration Synthesis on Block Copolymer Templates. *ACS Nano* **2011**, *5*, 4600−4606.
(97) Zhang, Q.; Matsuoka, F.; Suh, H. S.; Beaucage, P. A.; Xiong, S.; Smilgies, D. M.; Tan, K. W.; Werner, J. G.; Nealey, P. F.; Wiesner, U. B. Pathways to Mesoporous Resin/Carbon Thin Films with Alternating Gyroid Morphology. *ACS Nano* **2018**, *12*, 347−358.
(98) Jeong, J. W.; Park, W. I.; Do, L. M.; Park, J. H.; Kim, T. H.; Chae, G.; Jung, Y. S. Nanotransfer Printing with Sub-10 nm Resolution Realized Using Directed Self-Assembly. *Adv. Mater.* **2012**, *24*, 3526−3531.
(99) Kim, S. Y.; Nunns, A.; Gwyther, J.; Davis, R. L.; Manners, I.; Chaikin, P. M.; Register, R. A. Large-Area Nanosquare Arrays from Shear-Aligned Block Copolymer Thin Films. *Nano Lett.* **2014**, *14*, 5698−5705.
(100) Tavakkoli, K G A.; Gotrik, K. W.; Hannon, A. F.; Alexander-Katz, A.; Ross, C. A.; Berggren, K. K. Templating Three-Dimensional Self-Assembled Structures in Bilayer Block Copolymer Films. *Science* **2012**, *336*, 1294−1298.
(101) Tavakkoli, K. G. A.; Nicaise, S. M.; Gadelrab, K. R.; Alexander-Katz, A.; Ross, C. A.; Berggren, K. K. Multilayer Block Copolymer Meshes by Orthogonal Self-Assembly. *Nat. Commun.* **2016**, *7*, 10518.
(102) Rahman, A.; Majewski, P. W.; Doerk, G.; Black, C. T.; Yager, K. G. Non-Native Three-Dimensional Block Copolymer Morphologies. *Nat. Commun.* **2016**, *7*, 13988.
(103) Cha, S. K.; Lee, G. Y.; Mun, J. H.; Jin, H. M.; Moon, C. Y.; Kim, J. S.; Kim, K. H.; Jeong, S. J.; Kim, S. O. Self-Assembly of Complex Multimetal Nanostructures from Perforated Lamellar Block Copolymer Thin Films. *ACS Appl. Mater. Interfaces* **2017**, *9*, 15727−15732.
(104) Yager, K. G. SciAnalysis http://gisaxs.com/index.php/SciAnalysis (accessed Feb 22, 2020).
(105) Nečas, D.; Klapetek, P. Gwyddion: An Open-Source Software for SPM Data Analysis. *Cent. Eur. J. Phys.* **2012**, *10*, 181−188.

https://dx.doi.org/10.1021/acsnano.0c00696
ACS Nano 2020, 14, 4805−4815